Mitigating the Hubbard Sign Problem. A Novel Application of Machine Learning

Marcel Rodekamp[a,b,c,d,*] **and Christoph Gäntgen**[a,c,d]

[a]*Institute for Advanced Simulation, Forschungszentrum Jülich, 54245 Jülich, Germany*

[b]*JARA & Jülich Supercomputing Center, Forschungszentrum Jülich, 54245 Jülich, Germany*

[c]*Center for Advanced Simulation and Analytics (CASA), Forschungszentrum Jülich, 52425 Jülich, Germany*

[d]*Helmholtz-Institut für Strahlen- und Kernphysik, Rheinische Friedrich-Wilhelms-Universität Bonn, 53115 Bonn, Germany*

E-mail: m.rodekamp@fz-juelich.de, c.gaentgen@fz-juelich.de

Many fascinating systems suffer from a severe (complex action) sign problem preventing us from calculating them with Markov Chain Monte Carlo simulations. One promising method to alleviate the sign problem is the transformation of the integration domain towards Lefschetz Thimbles. Unfortunately, this suffers from poor scaling originating in numerically integrating of flow equations and evaluation of an induced Jacobian. In this proceedings we present a new preliminary Neural Network architecture based on complex-valued affine coupling layers. This network performs such a transformation efficiently, ultimately allowing simulation of systems with a severe sign problem. We test this method within the Hubbard Model at finite chemical potential, modelling strongly correlated electrons on a spatial lattice of ions.

---

*Speaker

1. Introduction

Markov Chain Monte Carlo algorithms (MCMC) enjoy great success in simulating many theories from the Ising model up to Lattice QCD. Albeit the potential, MCMC has a hard time whenever the action becomes complex-valued due to the associated Boltzmann weight loosing its interpretability as probability distribution.

Using MCMC, we focus on the Hubbard model capturing electronic properties of systems with strongly interacting electrons propagating on a fixed spatial lattice of ions. Examples for such systems are carbon nano structures like Graphene and Fullerene C_n. In the Hubbard model the sign problem is observed at finite chemical potential as well as on non-bipartite lattices[1]. Reweighting can treat the complex-valued Boltzmann weight though, at the same time, introducing an exponentially hard to estimate normalization.

Deforming the region of integration onto Manifolds with an almost constant imaginary action showed great promise in reducing the sign problem substantially [1–4]. Practically, this deformation requires numerical integration of differential equations which becomes infeasible for larger systems. We aim to identify efficient Neural Network architectures to learn such beneficial deformations. This removes the cost of numerically integrating configurations and enables simulations of large systems with a sign problem beyond the standard reweighting approach.

In this proceedings, we collect material from our earlier publications [5, 6] and a master thesis [7]. The manuscript is organized in the following way. In section 2 a brief introduction to the Hubbard model and the tested system is presented along a short discussion of the sign problem. This discussion is then followed by the definition of the neural network architectures as published in [5, 6]. Further, in section 3 correlator results are presented and we discuss the obtained charge density of one of the larger systems.

2. Formalism

The Hubbard model [8] describes a fixed spatial lattice X of ions on which electrons can move and interact. Its Hamiltonian, in particle-hole basis, is

$$\mathcal{H}[K, V, \mu] = - \sum_{x,y \in X} \left(p_x^\dagger K^{xy} p_y - h_x^\dagger K^{xy} h_y \right) + \frac{1}{2} \sum_{x,y \in X} \rho_x V^{xy} \rho_y + \mu \sum_{x \in X} \rho_x,$$

where the amplitudes in K encode the hopping of fermionic particles p and holes h, the potential V describes the interactions between charges

$$\rho_x = p_x^\dagger p_x - h_x^\dagger h_x \tag{1}$$

and the chemical potential μ incentivizes charge. By adjusting the hopping and lattice symmetry K as well as the interaction V this model can describe a wide variety of physical systems. In the following investigation, five systems are considered as displayed in figure 1. The 2 site system describes one unit cell of the honeycomb structure used for Graphene type models which we

---

[1]Bipartite describes lattice geometries at which the sites can be two coloured such that no neighbouring sites have the same colour. For example, the square is bipartite while the triangle is non-bipartite.
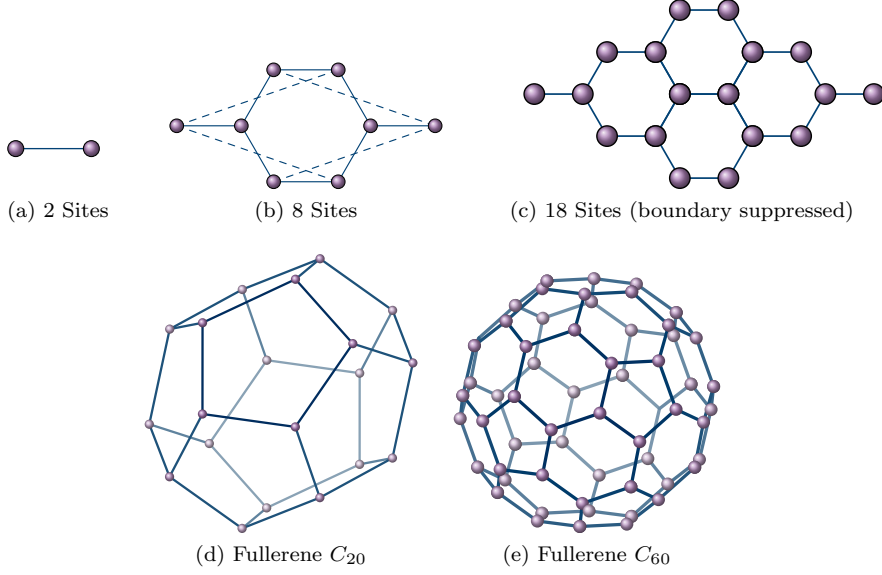
(a) 2 Sites   (b) 8 Sites   (c) 18 Sites (boundary suppressed)

(d) Fullerene C_{20} (e) Fullerene C_{60}

Figure 1: Showing the different geometries considered in this proceedings. Each vertex represents an ion and each (dashed) line depicts the nearest-neighbor hopping that is allowed by the Hubbard model. Dashed lines indicate periodic boundary condition where possible.

successively built up with the 8 and 18 site ones. Secondly, we present preliminary results for fullerenes C_{20} and C_{60} at zero chemical potential. In all cases K encodes nearest-neighbor hopping and we assume an on-site interaction,

$$K = \kappa \delta_{\langle xy \rangle} \qquad\qquad V = U\delta_{xy}. \qquad (2)$$

In figure 1 the sites, i.e. ions and their nearest neighbor connections are depicted. Lines stretching out display periodic boundary of the spatial lattice (suppress in the 18 site case).

2.1 Simulation Setup

Calculating observables follows the standard procedure [9] of evaluating the thermal trace. After trotterizing into N_t time slices, inserting Grassmannian resolutions of the identity and linearizing the interaction via the Hubbard-Stratonovich transformation [10] the Hamiltonian is transformed into the action

$$S[\Phi \,|\, K, V, \mu] = -\log \det\{M[\Phi \,|\, K, \mu] \cdot M[-\Phi \,|\, -K, -\mu]\} + \frac{1}{2}\sum_{t=0}^{N_t-1}\sum_{x,y\in X}\Phi_{tx}\delta V^{-1\,xy}\Phi_{ty}, \quad (3)$$

where $\Phi \in \mathbb{R}^{|\Lambda|}$ is an auxiliary field on the spacetime lattice $\Lambda = [0, N_t - 1] \otimes X$ and $\delta = \beta/N_t$ is the (temporal) lattice spacing controlled by the inverse temperature β. The fermion matrix is not uniquely defined on the lattice, we choose the exponential discretization [11]

$$M[\Phi \,|\, K, \mu]_{x't';xt} = \delta_{x'x}\delta_{t't} - \left(e^{\delta(K+\mu)}\right)_{x'x} e^{+i\Phi_{xt}}\mathcal{B}_{t'}\delta_{t'(t+1)} \qquad (4)$$

3

where $\mathcal{B}$ encodes the anti-periodic boundary conditions in time. For bipartite systems we may replace $-K$ with $+K$ in the holes' fermion matrix [9]. The thermal trace for this is expressed as path integral

$$\langle O \rangle = \frac{1}{\mathcal{Z}} \int \mathcal{D}\Phi \, e^{-S[\Phi]} O[\Phi] = \int \mathcal{D}\Phi \, p_S[\Phi] O[\Phi] \tag{5}$$

For cases of real action we can apply MCMC to generate N_{conf} configurations according to the Boltzmann distribution $p_S[\Phi]$ and estimate observables (5) by an unweighted expectation value. If the action is complex valued we apply reweighting

$$\langle O \rangle = \frac{\left\langle e^{-i\,\text{Im}\{S\}} O \right\rangle_{\text{Re}\{S\}}}{\left\langle e^{-i\,\text{Im}\{S\}} \right\rangle_{\text{Re}\{S\}}} = \frac{1}{\Sigma} \left\langle e^{-i\,\text{Im}\{S\}} O \right\rangle_{\text{Re}\{S\}}. \tag{6}$$

and sample configurations according to the Boltzmann distribution under the real part of the action. It has been shown [12] that an effective number of configurations

$$N_{\text{conf}}^{\text{eff}} = |\Sigma|^2 \cdot N_{\text{conf}} \tag{7}$$

controls the scaling of statistical errors $\sim \left(N_{\text{conf}}^{\text{eff}}\right)^{-1/2}$. This translates the sign problem to the ability of calculating the denominator Σ, i.e. the statistical power, reliably [5, 12–14].

A promising approach to mitigate, or even remove, the sign problem is to deform the region of integration $\Phi \in \mathcal{M}_\mathbb{R} = \mathbb{R}^{|\Lambda|}$ onto a manifold on which the imaginary part of the action is (nearly[2]) constant [2, 15], $\mathcal{M} = \left\{ \Phi \in \mathbb{C}^{|\Lambda|} \mid \text{Im}\{S[\Phi]\} = const. \right\}$. If $\mathcal{M}$ is in the same homology class as $\mathcal{M}_\mathbb{R}$ an analogue of the Cauchy integral theorem ensures that the observables are unchanged. Parametrizing fields $\Phi(\phi) \in \mathcal{M}$ then adds a Jacobian defining the used effective action

$$S_{\text{eff}}[\phi] = S[\Phi(\phi)] - \log \det\{J[\phi]\}, \quad J_{ij} = \frac{\partial \Phi(\phi)_i}{\partial \phi_j} \tag{8}$$

There are many strategies for picking target manifolds $\mathcal{M}$ [16]. One choice is to try to approximate the Lefschetz thimbles [15]. Each thimble contains a critical point Φ_{cr} that is a fixed point of the holomorphic flow

$$\frac{d\Phi(\tau)}{d\tau} = \pm \left(\frac{\partial S[\Phi(\tau)]}{\partial \Phi(\tau)} \right)^*, \quad \Phi(0) = \phi \tag{9}$$

introducing the fictitious flow time τ. A thimble is the set of complexified configurations that flow to a critical point under downward flow, i.e. $-$ in (9). An integrator for (9) will always be computationally expensive [2, 5, 6]. However, the non-interacting solution $\phi = 0$ for (9) assuming a constant field $\Phi_{t,x} = \Phi_{t',x'}$ defines a (hyper-) plane parallel to the real plane $\mathcal{M}_\mathbb{R}$ that goes through the main critical point $i\Phi_c^0$. This so called tangent plane $\mathcal{M}_T = \{\phi + i\Phi_c^0 \mid \forall \phi \in \mathcal{M}_\mathbb{R}\}$ showed promise in sufficiently mitigating the sign problem, at least for smaller systems [5, 6, 13, 17, 18].

---

[2]If $\text{Im}\{S\} \approx const$, the statistical power $|\Sigma| = \left| \left\langle e^{i\,\text{Im}\{S_{\text{eff}}\}} \right\rangle \right| \approx \left| \left\langle e^{i \cdot const} \right\rangle \right| \approx 1$ yielding nearly no reduction in effective number of configurations $N_{\text{conf}}^{\text{eff}} \approx N_{\text{conf}}$.

2.1.1 Neural Network Architectures

To improve beyond the tangent plane it seems plausible to identify a transformation that transforms a given configuration $\phi \in \mathcal{M}_{\mathbb{R}}$ to a target manifold $\tilde{\mathcal{M}}$ that may be closer to $\mathcal{M}$ than the tangent plane. Such a transformation may be parametrized by a neural network

$$\text{SHIFT} : \mathcal{M}_{\mathbb{R}} \to \tilde{\mathcal{M}}, \ \phi \mapsto \phi + i\left(\Phi_c^0 + NN(\phi)\right). \tag{10}$$

For the neural network part NN we pick two linear layers $\omega\phi + b$ with real trainable weights ω and biases b which are separated by a leacky-ReLU. As the effective action (8) suggests the defining transformations Jacobian needs to be computed

$$\log \det\{J_{\text{SHIFT}}[\phi]\} = \log \det\left\{\mathbb{1} + i\frac{\partial NN(\phi)}{\partial \phi}\right\} \tag{11}$$

which requires an $O(V^3)$ algorithm for the determinant calculation. This scaling is not feasible for large scale systems but still much cheaper than applying a Runge-Kutta — or similar algorithms — to integrate the holomorphic flow equations.

To improve the scaling, we identify a neural network that has a cheaper determinant. One such architectures is given by Affine Coupling Layers [19, 20] that approximate the integrator $\Phi(\phi) \approx \mathcal{NN}(\phi)$

$$\mathcal{NN}_\ell(\Phi) = \begin{cases} c_\ell\left[\Phi_A, \Phi_B\right] & A_\ell \text{ components} \\ \Phi_B & B_\ell \text{ components} \end{cases} \tag{12}$$

Here A and B are layer-specific partitions of the input vector Φ of equal cardinality $1/2|\Lambda|$. $\Phi_{A,B}$ are the components of the input belonging to the indicated partition. We apply the affine coupling [19]

$$c_\ell\left[\Phi_A, \Phi_B\right] = e^{m_\ell(\Phi_B)} \odot \Phi_A + a_\ell(\Phi_B). \tag{13}$$

The coupling functions $m_\ell, a_\ell : \mathbb{C}^{|\Lambda|/2} \to \mathbb{C}^{|\Lambda|/2}$ are again two linear layers separated by the non-linear Softsign function. To ensure that the neural network produces a complex configuration as is required by the holomorphic flow, the weights and biases need to be complex valued which is discussed in more detail in [6]. A single layer just transforms half of the configuration, we thus pair it up with a second layer that is set up in the same way but with the roles of A and B interchanged. This setup allows to express the Jacobian, with $L/2$ of these pairs, in the form

$$\log \det\{J_{\mathcal{NN}}(\phi)\} = \sum_{\ell=1}^{L} \sum_{i=0}^{|A|-1} m_\ell\left(\Phi_{\ell-1}(\phi)_B\right)_i. \tag{14}$$

which adds only an $O(V)$ cost to the application of the transformation.

For any of these architectures we perform Molecular Dynamics on $\mathcal{M}_{\mathbb{R}}$ using a standard leapfrog algorithm and then apply the network to move onto $\tilde{\mathcal{M}}$. Accept/Reject is then performed according to the effective action (8) using the transformed configuration from the Network and the Jacobian defined by the network. This machine learning enhanced Hybrid Monte Carlo is referred to as ML HMC.

2.2 Observables

We are interested in the electronic properties of a given system. Euclidean correlation functions of a single particle or a single hole

$$C_{xy}^{\stackrel{p}{h}}(t) = \left\langle p_x^\dagger(t)p_y(0) \right\rangle = \left\langle M[\pm\Phi| \pm K, \pm\mu]_{xt;y0}^{-1} \right\rangle, \tag{15}$$

momentum projected and averaged we obtain $C_{sp}(t)$ [6]. In the future we aim to match the parameters $U/\kappa, \mu$ to real-world systems and extract the band-gap $C_{xy}(t) \sim e^{-t \cdot \Delta E}$. Further, the charge density is defined by

$$\rho(\mu) = \frac{1}{|X|} \sum_{x \in X} \langle\rho_x\rangle = \frac{1}{|X|} \sum_{x \in X} C_{x,x}^p(0) - C_{x,x}^h(0). \tag{16}$$

It is point symmetric around the electric neutral half-filling point, $\mu = 0$, due to particle-hole symmetry. For very large $\mu \to \pm\infty$ the charges (+) or holes (-) are favoured yielding a charge density of ± 1. Qualitatively, it is expected that the system's charge equals integer multiples of the electric charge $n \cdot e^-$ with $n \in [-N_x, N_x]$, i.e. $\rho(\mu) = n/N_x$.

3. Numerical Results

We experimented with different training setups. Foremost, supervised training using ADAM to minimize the $L1-$Loss. The training data consists out of $O(10\,000)$ pairs $(\phi, \Phi(\phi))$ obtained by a Runge-Kutta of 4th order. For further details consider [5, 6].

In figure 2 correlators for systems with 2 and 8 sites are compared using the different algorithms HMC (red) — on the tangent plane — ML HMC (blue), applying the coupling network $\mathcal{NN}$, and exact diagonalization (black) [6]. We use $N_\text{conf} \in \{1000, 100\,000\}$ to portray the effect of the statistical power on the effective number of configurations. Corresponding statistical powers $|\Sigma|$ can be found in [6]. The system parameters — $N_t = 32$, $\beta = 4$, $U = 4$ and $\mu = 3$ — are kept fix. The ML HMC outperforms the HMC in terms of signal. The 8 site system has a stronger sign problem to an extend that HMC retrieves no signal. If a signal is obtained, both algorithms agree with the exact diagonalization. In figure 3 the correlators for the system with 18 sites are displayed [6]. The system is computed at $N_t = 32$, $\beta = 4$, $U = 3$ and $\mu = 3$. The sign problem is much stronger than in the previous cases due to the larger volume. Nevertheless the ML HMC extracts a good signal for the correlators. Similar to the 8 site case HMC can't keep up. Due to the number of sites exact diagonalization is not feasible.

Continuing the 18 site model — with $U = 2$, $\beta = 5$, $N_t = 32$ — we want to study the charge density (16) subjected to the chemical potential. This can be seen in figure 4 [7]. We compare tangent plane HMC (red) and ML HMC (blue) using the SHIFT network. Varying the chemical potential has shown that for small and large values the sign problem is mild (on the tangent plane). However, in the intermediate range of $\mu \in [2, 3]$ the tangent plane is not sufficient for a reasonable estimate, where we apply ML HMC with the SHIFT network. The point at $\mu = 2.5$ requires more attention and we plan to address it with the coupling network in the future expecting much better results. The expected behaviour of the charge density, $\rho(\mu = 0) = 0$ and $\rho(\mu \to \infty) \to 1$, is found numerically. The dashed line exemplarily indicates an expected plateau at $\langle\rho(\mu)\rangle = 4/18$. As it can
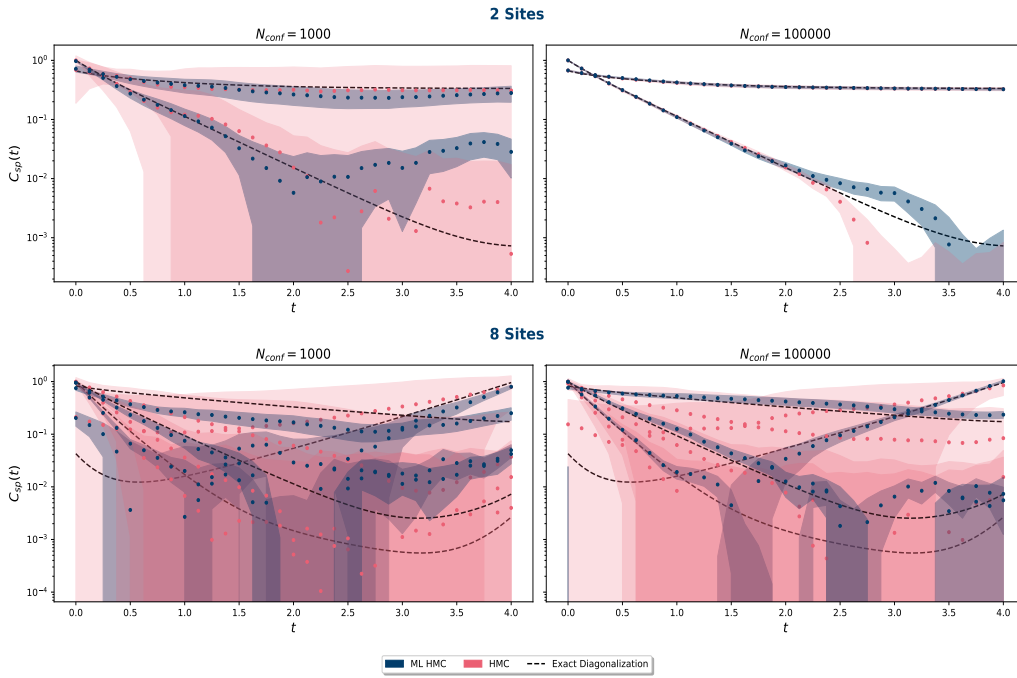
Figure 2: Each row in this figure shows the correlators of a system with 2 (upper row) and 8 (lower row) sites [6]. The different columns correspond to a number of configurations, $N_{conf} \in \{1000, 100\,000\}$, used to estimate the correlators. Three methods — ML HMC with coupling layer $\mathcal{NN}$ (blue), HMC on the Tangent Plane (red) and exact diagonalization (black) — are compared to show the effectiveness and correctness of the introduced machine learning enhanced method. The sign problem manifests as a loss of signal, i.e. small number of effective configurations N_{conf}^{eff} (7), and greatly increases as the number of sites expands. It can be seen that the ML HMC has a substantially reduced sign problem.
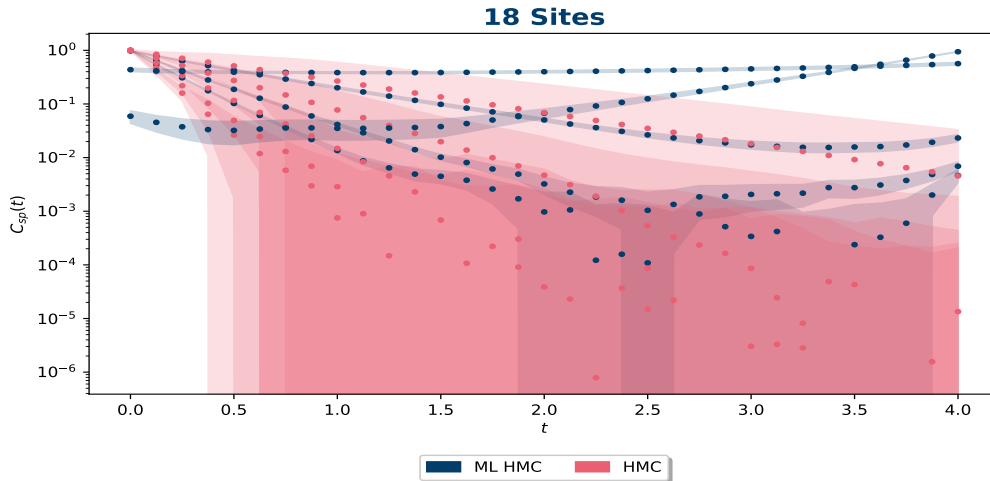
Figure 3: The correlators of Graphene with 18 ions are shown [6]. 100 000 measurements are taken. With this larger lattice direct diagonalization as in figure 2 is not tractable any more hence only the two statistical methods ML HMC using the coupling network $\mathcal{NN}$ (blue) and HMC on the tangent plane (red) are compared. As expected the ML HMC improves the signal drastically.
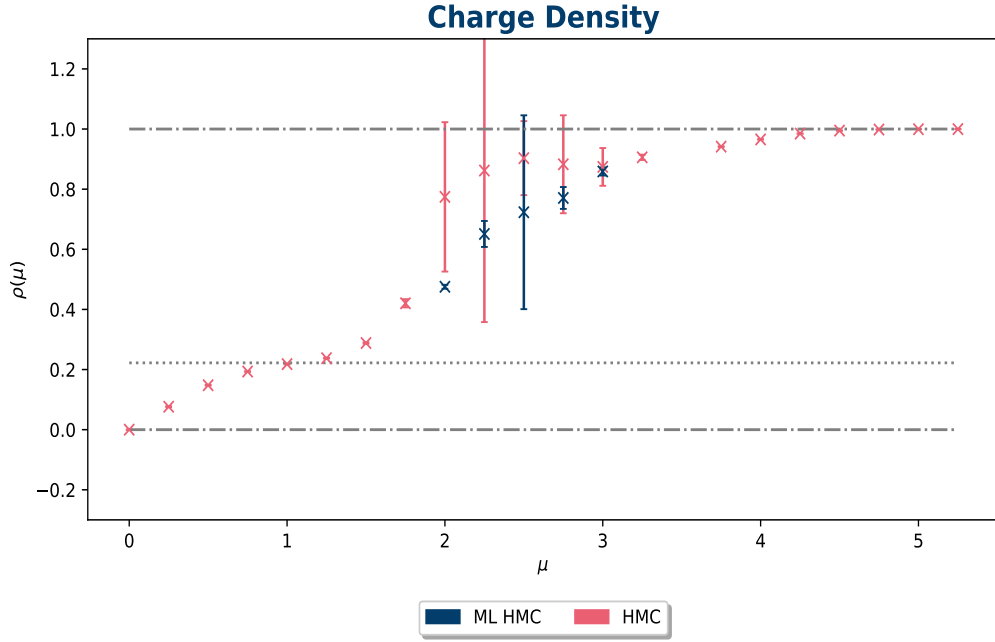
Figure 4: We computed the charge density for several values of the chemical potential $\mu \in [0, 5.2]$ for an 18 site Graphene sheet [7]. For most smaller and larger values of μ the sign problem is small enough that estimation with HMC on the tangent plane (red) is sufficient. However, in the region $\mu \in [2, 3]$ an ML HMC (blue) is used to narrow particular values for which the sign problem becomes untraceable. The features at $\mu = 0$ and $\mu \to \infty$ are captured as expected. Finding the charge plateaus at $\rho(\mu) \sim n$, however, is yet unavailable due to the small β. The dashed line at $\rho(\mu) = 4/18$ indicate an expected plateau which may be surmised around $\mu \approx 1$.
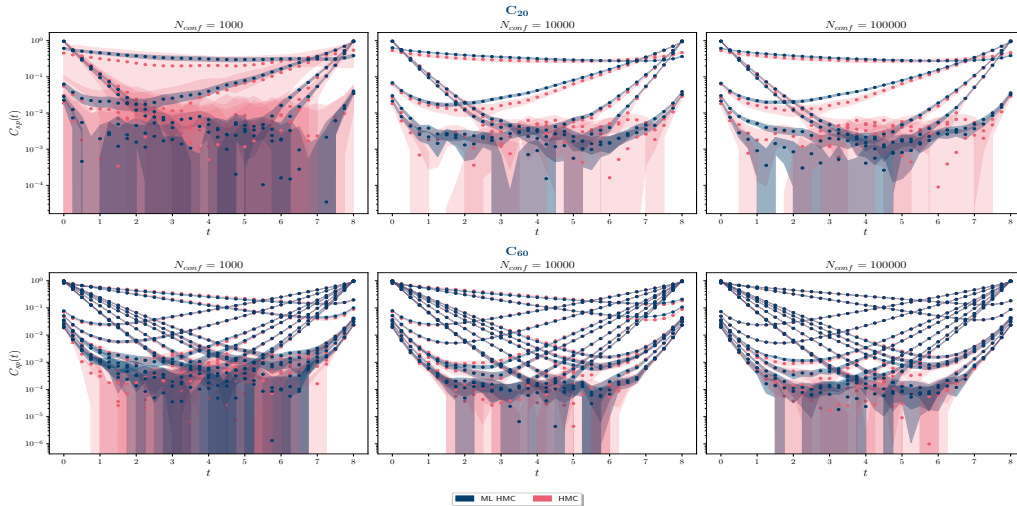

Figure 5: The correlators of Fullerene C_{20} (upper row) and C_{60} (lower row) are shown. A real plane (red) and a tangent plane (blue) HMC at inverse temperature $\beta = 8$ and $N_t = 32$ time slices are compared. We consider an on-site interaction $U = 3$ and zero chemical potential. The, here negligible, sign problem solely stems from the non-bipartiteness of the system due to the pentagonal rings. Already, at small number of configurations $N_{conf} \leq 10\,000$ the signals are very good.

be seen, this plateau is not fully deducible but may be surmised around $\mu \approx 1$. Studies of smaller systems, see [7], indicate increasing β makes these plateaus more pronounced.

To probe our method in physically more relevant systems than the 18 Site Graphene sheet, we started an investigation of Fullerene C_{20} and C_{60}. The correlators at $N_t = 32$, $\beta = 8$, $U = 3$ and zero chemical potential are displayed in figure 5. The mild sign problem is solely due to the non-bipartiteness of the lattice structure. We compare standard HMC (red) with tangent plane HMC (blue) to show that the tangent plane obtains a good signal already at small number of configurations $N_{conf} = 1000$ in both systems. For C_{60} the sign problem is negligible and the real plane HMC gives a good signal too. For finite chemical potential the sign problem aggravates as it imposes a second source. We are currently working on this particular lattice geometry.

4. Conclusions

Simulating systems with strongly correlated electrons is a rather challenging task due to the innate sign problem for doped systems. Current methods, like deformation onto Lefschetz thimbles, suffer from a very difficult scaling in computational cost. We overcome this issue by identifying efficient Neural Network architectures and incorporating them in a HMC algorithm. We present first studies of doped Graphene sheets using this enhanced HMC and demonstrate a substantial improvement of the signal, effectively mitigating the sign problem. Considering systems with increasing volume illustrates some stability of this method for larger volumes. Further, preliminary simulation of Fullerene C_{20} and C_{60} at vanishing chemical potential are shown. In the near future we will apply the neural network enhanced HMC also at finite chemical potential.

Acknowledgments

References

[1] K. Kashiwa, Y. Mori, and A. Ohnishi, Phys. Rev. D **99**, 014033 (2019), arXiv:1805.08940 [hep-ph] .

[2] A. Alexandru, G. Basar, P. F. Bedaque, and N. C. Warrington, Rev. Mod. Phys. **94**, 015006 (2022).

[3] W. Detmold, G. Kanwar, M. L. Wagman, and N. C. Warrington, Phys. Rev. D **102**, 014514 (2020).

[4] W. Detmold, G. Kanwar, H. Lamm, M. L. Wagman, and N. C. Warrington, Phys. Rev. D **103**, 094517 (2021), arXiv:2101.12668 [hep-lat] .

[5] J.-L. Wynen, E. Berkowitz, S. Krieg, T. Luu, and J. Ostmeyer, Physical Review B **103**, 125153 (2021).

[6] M. Rodekamp, E. Berkowitz, C. Gäntgen, S. Krieg, T. Luu, and J. Ostmeyer, Phys. Rev. B **106**, 125139 (2022).

[7] C. Gäntgen, "Investigating doped systems with holomorphic flow and machine learning," (2021), access upon request (`c.gaentgen@fz-juelich.de`).

[8] J. Hubbard, Proceedings of the Royal Society of London. Series A, Mathematical and Physical Sciences **276**, 238 (1963).

[9] R. Brower, C. Rebbi, and D. Schaich, (2012), 10.48550/ARXIV.1204.5424.

[10] J. Hubbard, Phys. Rev. Lett. **3**, 77 (1959).

[11] J.-L. Wynen, E. Berkowitz, C. Körber, T. A. Lähde, and T. Luu, Physical Review B **100**, 075141 (2019).

[12] C. E. Berger, L. Rammelmüller, A. C. Loheac, F. Ehmann, J. Braun, and J. E. Drut, Physics Reports **892**, 1 (2021).

[13] A. Alexandru, G. Başar, and P. Bedaque, Physical Review D **93**, 014504 (2016).

[14] Y. Mori, K. Kashiwa, and A. Ohnishi, Physics Letters B **781**, 688 (2018).

[15] M. Cristoforetti, F. Di Renzo, L. Scorzato, A. Collaboration, *et al.*, Physical Review D **86**, 074506 (2012).

[16] Y. Tanizaki, H. Nishimura, and J. J. M. Verbaarschot, JHEP **10**, 100 (2017), arXiv:1706.03822 [hep-lat] .

[17] A. Alexandru, P. F. Bedaque, H. Lamm, S. Lawrence, and N. C. Warrington, Phys. Rev. Lett. **121**, 191602 (2018), arXiv:1808.09799 [hep-lat] .

[18] N. C. Warrington, *Taming the Sign Problem in Lattice Field Theory With Deformed Path Integral Contours*, Ph.D. thesis, Maryland U. (2019).

[19] M. S. Albergo, D. Boyda, D. C. Hackett, G. Kanwar, K. Cranmer, S. Racanière, D. J. Rezende, and P. E. Shanahan, arXiv preprint arXiv:2101.08176 (2021).

[20] S. Foreman, T. Izubuchi, L. Jin, X.-Y. Jin, J. C. Osborn, and A. Tomiya, arXiv preprint arXiv:2112.01586 (2021).